

Crystal Structure of the Catalytic Domains of Adenylyl Cyclase in a Complex with $G_{s\alpha}$ ·GTP γ S

John J. G. Tesmer, Roger K. Sunahara, Alfred G. Gilman, Stephen R. Sprang

The crystal structure of a soluble, catalytically active form of adenylyl cyclase in a complex with its stimulatory heterotrimeric G protein α subunit ($G_{s\alpha}$) and forskolin was determined to a resolution of 2.3 angstroms. When P-site inhibitors were soaked into native crystals of the complex, the active site of adenylyl cyclase was located and structural elements important for substrate recognition and catalysis were identified. On the basis of these and other structures, a molecular mechanism is proposed for the activation of adenylyl cyclase by $G_{s\alpha}$.

Adenylyl cyclase is the effector enzyme responsible for converting adenosine triphosphate (ATP) to adenosine 3,5-monophosphate (cAMP), a ubiquitous second messenger that mediates diverse cellular responses primarily by activating cAMP-dependent protein kinases. Nine isoforms of adenylyl cyclase have been identified (ACI through ACIX). These proteins share several regulatory features: activation by the α subunit of the heterotrimeric G protein G_s , activation by the diterpene forskolin, and inhibition by a class of adenosine analogs known as P-site inhibitors. The activity of individual isoforms can also be regulated by other G protein subunits, Ca^{2+} -calmodulin, Ca^{2+} , or phosphorylation (1–3). This regulatory diversity allows each isoform of adenylyl cyclase to respond to intercellular and intracellular signals in a manner appropriate for its cellular context.

The first cDNA encoding a mammalian adenylyl cyclase revealed a protein of structural complexity commensurate with the difficulties encountered in its purification and expression (4). Adenylyl cyclase has a short cytosolic amino terminus, followed by two repeats of a module composed of a hydrophobic domain, modeled as six transmembrane helices, followed by a ~40-kD cytosolic domain. Each of the two cytoplasmic domains, designated C_1 and C_2 , respectively, contains a region of ~200 amino acid residues (C_{1a} , C_{2a}) that is homologous between C_1 and C_2 and among all isoforms

of the enzyme. Similar domains are also found in membrane-bound and soluble guanylyl cyclases (5).

The cytosolic domains of adenylyl cyclase are implicated in catalysis. The C_{1a} and C_{2a} domains from the same or from different isoforms of adenylyl cyclase can be expressed in bacteria as 50-kD fusion proteins that retain high enzymatic activity (6, 7). The individual domains can also be expressed and purified as 25-kD proteins (8, 9). Although these individual domains form homodimers that retain little or no catalytic activity, adenylyl cyclase activity is restored when they are mixed. The cytosolic domains also retain the common regulatory properties of adenylyl cyclases (6, 8–10).

We overexpressed and purified the C_{1a} domain from adenylyl cyclase V (VC_1) and the C_2 domain from adenylyl cyclase II (IIC_2). The apparent affinity of VC_1 for IIC_2 is weak ($>10 \mu M$), and the basal catalytic activity of their complex is low ($\sim 100 \text{ nmol min}^{-1} \text{ mg}^{-1}$). In the presence of forskolin or guanosine 5'-O-(3-thiotriphosphate)-activated $G_{s\alpha}$ ($G_{s\alpha}$ ·GTP γ S), or both, the apparent affinity of VC_1 for IIC_2 and their catalytic activity increase (dissociation constant $K_d = 150 \text{ nM}$, specific activity $\geq 150 \mu \text{mol min}^{-1} \text{ mg}^{-1}$) (11). Activators of adenylyl cyclase thus appear to facilitate interactions between the two cytosolic domains and stimulate catalysis. Data from sedimentation equilibrium, gel filtration, and equilibrium dialysis studies indicate that the forskolin- and $G_{s\alpha}$ -activated complex contains one molecule each of VC_1 , IIC_2 , $G_{s\alpha}$ ·GTP γ S, and forskolin (11, 12). The activated complex is able to bind one molecule of a nonhydrolyzable ATP analog, Ap(CH₂)pp, presumably at the interface between the C_1 and C_2 domains. Like native adenylyl cyclase, the VC_1 · IIC_2 complex is inhibited by P-site inhibitors, a

class of compounds that includes 2'-deoxyadenosine and its 3' mono- or polyphosphates (13). These compounds are noncompetitive or uncompetitive inhibitors with respect to ATP, and they bind with highest apparent affinity to the activated enzyme and only in the presence of pyrophosphate. The VC_1 and IIC_2 domains are also amenable to structural analysis, as demonstrated below and by the crystal structure of the IIC_2 homodimer (14). Although the IIC_2 homodimer has little or no enzymatic activity, its structure provides a model for the C_1 · C_2 heterodimer and demonstrates how forskolin binds within and stabilizes the C_1 · C_2 interface.

We now present the structure of activated $G_{s\alpha}$ alone [described in a companion paper (15)] and the structure of $G_{s\alpha}$ associated in a quaternary complex with VC_1 , IIC_2 , and forskolin. We also determined the structure of this forskolin-bound heterotrimer in a complex with the P-site inhibitor 2'-deoxy-3'-adenosine monophosphate (2',d3'-AMP) and pyrophosphate, which provides direct insight into the mechanism of catalysis and the structural mechanism of P-site inhibition. Taken together, these structures also permit us to propose a molecular mechanism for activation of adenylyl cyclase by $G_{s\alpha}$.

Structure determination. Bovine $G_{s\alpha}$ ·GTP γ S·Mg²⁺ was crystallized in a ternary complex with a C_1 fragment of canine ACV (residues 364 to 580) (VC_1) and a C_2 fragment of rat ACII (residues 874 to 1081) (IIC_2) in the presence of 7-deacetyl-7-(O-N-methylpiperazino)- γ -butyryl forskolin (MPFsk) (16). We used the short alternative splice form of $G_{s\alpha}$ (17), which was synthesized in *Escherichia coli* with a carboxyl-terminal hexahistidine tag and purified as described (11). The recombinant $G_{s\alpha}$ contains no lipid modifications. VC_1 , which has an NH₂-terminal hexahistidine tag, and IIC_2 were also produced in *E. coli* (8, 18). Before being crystallized, the quaternary complex of $G_{s\alpha}$, VC_1 , IIC_2 , and forskolin was purified by gel exclusion chromatography (11).

Crystals of $G_{s\alpha}$ · VC_1 · IIC_2 grow as 10- to 20- μm -thick plates and belong to space group $P2_12_12_1$ (Table 1). There is one complex per asymmetric unit of the crystal. Diffraction is anisotropic, such that data normal to the plate (the a^*b^* plane) extend only to 3.9 Å spacings, compared with a diffraction limit of 2.3 Å in the a^* and b^* directions. Therefore, reflections with $|l| > 18$, corresponding to spacings less than 3.9 Å in the direction along c^* , were removed from the data set before scaling. To prepare complexes with P-site inhibitors, we soaked crystals in a harvesting solution containing pyrophosphate and either 2',d3'-AMP or 2'-deoxy-3'-ATP (2',d3'-

J. J. G. Tesmer and S. R. Sprang are at the Howard Hughes Medical Institute and the Department of Biochemistry, The University of Texas Southwestern Medical Center, 5323 Harry Hines Boulevard, Dallas, TX 75235-9050, USA. R. K. Sunahara and A. G. Gilman are in the Department of Pharmacology, University of Texas Southwestern Medical Center, 5323 Harry Hines Boulevard, Dallas, TX 75235-9041, USA.

*To whom correspondence should be addressed. E-mail: sprang@howie.swmed.edu

ATP). After exposure to P-site inhibitors, crystals displayed increased mosaicity and concomitant reduction in the maximum limit of diffraction to 2.8 Å spacings in the a^* and b^* directions. Attempts to cocrystallize $G_{\text{src}} \cdot VC_1 \cdot IIC_2$ with either P-site inhibitors or $Ap(CH_2)_2pp$ have so far been unsuccessful. Complete data sets extending to 2.3 and 2.8 Å diffraction spacings were recorded at the Cornell High Energy Synchrotron Source (CHESS) for the $G_{\text{src}} \cdot VC_1 \cdot IIC_2$ complexes in the absence and presence of P-site inhibitors, respectively (Table 1).

We determined the structure of the $G_{\text{src}} \cdot VC_1 \cdot IIC_2$ complex by molecular replacement using the structure of $G_{\text{src}} \cdot IIC_2$ (19) and the IIC_2 homodimer (14) as search models. After several cycles of manual model reconstruction and refinement, the con-

ventional R factor was 22% and the free R factor (20) was 28%. Difference Fourier analysis revealed substantial conformational changes upon introduction of either of the two P-site inhibitors and pyrophosphate. These changes were primarily confined to two segments of polypeptide chain in VC_1 and the COOH-terminal β -ribbon of IIC_2 . The atomic model was revised in accordance with difference maps, and after subsequent refinement of this model, the P-site inhibitor, pyrophosphate, and Mg^{2+} could be discerned in difference density maps. The model of the complex containing MPFsk, 2',d3'-AMP, and pyrophosphate has been refined to conventional and free R factors of 24 and 32%, respectively.

All three proteins in the $G_{\text{src}} \cdot VC_1 \cdot IIC_2$ complex are disordered at their NH_2 - and

COOH-termini. The refined structure of G_{src} spans residues 36 to 393 (394 is the COOH-terminal residue; residue numbering is for the long splice variant of G_{src}). However, no electron density is observed for five residues in the linker 1 segment between residues 66 and 86 (alternative splicing excludes 14 of the residues in this range from the long form of G_{src}). The atomic model of VC_1 spans residues 376 to 565, and the structure of IIC_2 is well ordered between residues 879 and 1077 except for residues 954 to 963 in its $\beta 3' \text{--} \alpha 3'$ loop.

Structure of the $VC_1 \cdot IIC_2$ complex. As expected from their amino acid sequences, the tertiary structures of IIC_2 and VC_1 are almost identical (Fig. 1), and the overall quaternary structure of the $VC_1 \cdot IIC_2$ heterodimer is similar to that of the IIC_2 homodimer (14), although the two domains are rotated by 7° with respect to each other (see below). Secondary structure elements of IIC_2 are identified according to the convention of Zhang *et al.* (14) but are primed to distinguish them from the analogous structures in VC_1 . The surface of the heterodimer perpendicular to the pseudo two-fold axis (Fig. 1A) is denoted the ventral surface (14). A long, shallow trough running diagonally across this face of the heterodimer contains the forskolin and substrate binding sites. In contrast, extensive contacts between IIC_2 and VC_1 would appear to restrict access of substrates to their binding sites from the opposite, dorsal surface. In part because the NH_2 -termini of VC_1 and IIC_2 project away from the dorsal surface of the heterodimer, we propose that this surface faces the membrane. Nevertheless, because parts of the segments that connect the cytosolic to the membrane-spanning domains are either not present in our constructs or are disordered, alternative orientations are possible.

VC_1 and IIC_2 superimpose with a root-mean-square deviation (rmsd) of 1.3 Å for 153 structurally equivalent $C\alpha$ atom pairs. There are several notable structural differences between the domains. The first of these is found by comparing $\beta 1 \text{--} \alpha 1 \text{--} \alpha 2$ with $\beta 1' \text{--} \alpha 1' \text{--} \alpha 2'$ (Fig. 1B). The COOH-terminus of strand $\beta 1$ is two residues longer than $\beta 1'$ and is followed by a four-residue type I turn. In contrast, $\beta 1'$ is followed by a three-residue 3_{10} turn. Helix $\alpha 1$ is longer than $\alpha 1'$ by one helical turn and begins one residue earlier in the primary structure. Whereas $\alpha 1$ and $\alpha 2$ are connected by a common helical hairpin turn, the polypeptide chain succeeding $\alpha 1'$ forms a four-residue β -like extension, followed by a 3_{10} and then a left-handed helical turn before entering the $\alpha 2'$ helix. The more complex $\alpha 1' \text{--} \alpha 2'$ loop is partially the consequence of a four-residue insertion in the primary structure of IIC_2

Table 1. Summary of data collection and refinement statistics. Diffraction data from crystals of the $VC_1 \cdot IIC_2 \cdot G_{\text{src}}$ complex (16) were measured on a 1k by 1k ADSC charge-coupled-device area detector with 0.908 Å radiation from the A1 beamline at CHESS. All crystals were flash frozen in nitrogen-cooled liquid ethane on 0.2-mm cryoloops (Hampton) and were maintained throughout data collection in a cryostream at -180°C . With a 0.2-mm collimator, the mosaicity for native crystals of the complex was 0.5°, whereas those for the P-site complexes were typically 1.0°. Diffraction amplitudes from crystals of the complex were indexed and integrated with DENZO and scaled with SCALEPACK (44). Because the diffraction was anisotropic, reflections with l indices that had an absolute value greater than 18, corresponding to a 3.9 Å resolution cutoff along the c^* axis, were removed before scaling; the average l/σ , for the omitted reflections after scaling was 1.7. The structure of the complex was initially solved by molecular replacement, using the AMORE program (45) as implemented by the CCP4 program package (46), with 3.5 Å data collected by using $CuK\alpha$ radiation on a MacScience 2030DIP area detector. The unmodified structure of $G_{\text{src}} \cdot GTP \cdot \gamma S$ (19) served as the search model for G_{src} and that of the IIC_2 homodimer (14) served as the search model for the $VC_1 \cdot IIC_2$ heterodimer. The initial model for the native complex was built in O (47), and all subsequent refinement steps were performed with X-PLOR (48). Anisotropic overall B -factors (Aniso. B -factor) and a bulk solvent mask were used throughout the final rounds of refinement and model building. After convergence of the native structure, a difference Fourier map was used to reveal conformational changes in the complex containing P-site inhibitors. The polypeptide backbone was altered accordingly, and after refinement, weak but interpretable difference density was observed for the P-site inhibitor, pyrophosphate, and magnesium. After addition of these molecules to the atomic model, the P-site complex was subsequently refined and rebuilt through several more cycles. A total of 91% of the amino acids in the native complex and 87% of the amino acids in the P-site inhibited complex are found in the most favored regions, and none are found in disallowed regions of the Ramachandran plot (49).

Crystal	Native	2',d3'-AMP
Cell constants (Å)	$a=119.1, b=134.1, c=70.7$	$a=119.1, b=134.4, c=70.9$
No. of crystals	1	2
D_{min} (Å)	2.3 (along a^* and b^*)	2.8 (along a^* and b^*)
Unique reflections	37,320 (48,048)*	23,679 (25,919)*
Average redundancy	3.3 (3.1)*	3.3 (3.2)*
R_{sym} † (%)	9.5 (11.6)*	17.3 (17.8)*
Completeness (%)	75.1 (96.7)*	82.5 (90.3)*
$\langle l \rangle / \langle \sigma \rangle$	11.5 (8.6)*	6.4 (5.6)*
Resolution range for refinement (Å)	15 to 2.3	15 to 2.8
Number of protein atoms	5740	5724
Number of water molecules	70	0
Number of heterogen atoms	72	95
Rmsd bond lengths (Å)	0.007	0.010
Rmsd bond angles (°)	1.3	1.6
Rmsd bonded B -factors (Å ²)	3.9	4.5
$R_{\text{work}} \ddagger$ (%)	22	24
$R_{\text{free}} \S$ (%)	28	32
Aniso. B -factor ($B_{11} B_{22} B_{33}$) (Å ²)	-15, -24, 40	-10.1, -12.5, 22.6
Average B -factor (Å ²)	52.2	20.5

*Numbers in parentheses correspond to the complete data set before truncation. † $R_{\text{sym}} = \sum_h \sum_l |I(h) - I(h)| / \sum_h \sum_l I(h)$, where $I(h)$ is the mean intensity after rejections. ‡ $R_{\text{work}} = \sum_n \|F_{\text{obs}}(h) - |F_{\text{calc}}(h)|\| / \sum_n F_{\text{obs}}(h)$, where $F_{\text{obs}}(h)$ and $F_{\text{calc}}(h)$ are the observed and calculated structure factors, respectively; no l/σ cutoff was used. §Ten percent of the complete data set was excluded from refinement to calculate R_{free} . D_{min} = the minimum spacing of the integrated diffraction data.

relative to VC₁ (Fig. 2). The structural differences between these elements reflect their distinct functional roles. We show below that the turn at the NH₂-terminus of α 1 forms a P-loop-like structure that binds pyrophosphate, whereas the α 1'- α 2' loop forms part of the G_{s α} binding site.

Among the C₂ domains of adenylyl cyclase isoforms, the β 3'- α 3' loop is a site of sequence length variation (Fig. 2). This loop is poorly ordered in the crystal structures of both the IIC₂ homodimer and the G_{s α} -VC₁-IIC₂ heterotrimer. Sequences within the loop and the succeeding helix have been implicated in the interaction of adenylyl cyclase with the $\beta\gamma$ subunits of heterotrimeric G proteins (21), although if $\beta\gamma$ binds this peptide in the manner proposed (22), it would be upside-down with respect to the membrane if the dorsal surface of VC₁-IIC₂ faces the membrane as suggested above. In VC₁, the β 3- α 3 loop is an ordered seven-residue turn that contains the only *cis*-proline observed in either VC₁ or IIC₂.

The structural similarity between VC₁ and IIC₂ breaks down at a point that corresponds to the COOH-terminus of β 7 (middle of β 7') (Fig. 2) but resumes at the COOH-terminus of α 7 (NH₂-terminus of β 8'). In IIC₂, β 7' and β 8' form a long β ribbon in which the two strands are connected by a simple reverse turn (Fig. 1B). The end of the ribbon passes over the ventral channel of the VC₁-IIC₂ heterodimer and forms part of the P-site inhibitor-pyrophosphate binding site (see below). This region is disordered in the crystal structure of the IIC₂ homodimer (14). Strand β 7 of VC₁ is much shorter than its counterpart in IIC₂. In place of the β ribbon is a compact Ω loop (23) that contains two short α helices. The loop does not participate in G_{s α} or P-site inhibitor binding. Although the primary structure is not conserved between C₁ and C₂ in this region, it is maintained between corresponding domains in most adenylyl and guanylyl cyclase isoforms. Therefore, this COOH-terminal sub-

domain may participate in regulatory interactions that are unique to C₁ or C₂.

The VC₁-IIC₂ domain interface. The interface between VC₁ and IIC₂ buries more than 3300 Å² of solvent-accessible surface area (24). Including the molecule of MPFsk, a total of 4200 Å² of surface area is buried upon forming the VC₁-IIC₂-MPFsk complex. The pseudo-twofold symmetry of VC₁-IIC₂ is evident in their interface. Interfacial contacts (defined by interatomic distances of less than 4.0 Å) involve 28 residues in VC₁ and 33 residues in IIC₂. Only 17 of these residues from each domain are found at structurally equivalent positions. Of these residues, only 12 are conserved between C₁ and C₂ (Fig. 2).

There are two pseudosymmetric regions that form the VC₁-IIC₂ interface (Fig. 1C). In the first and much more extensive of these, closest to G_{s α} (upper right-hand side of Fig. 1C), β 2' of IIC₂ stacks on top of the β 4- β 5 loop of VC₁. The α 2' helix contacts the NH₂-terminal segment of β 1 and the

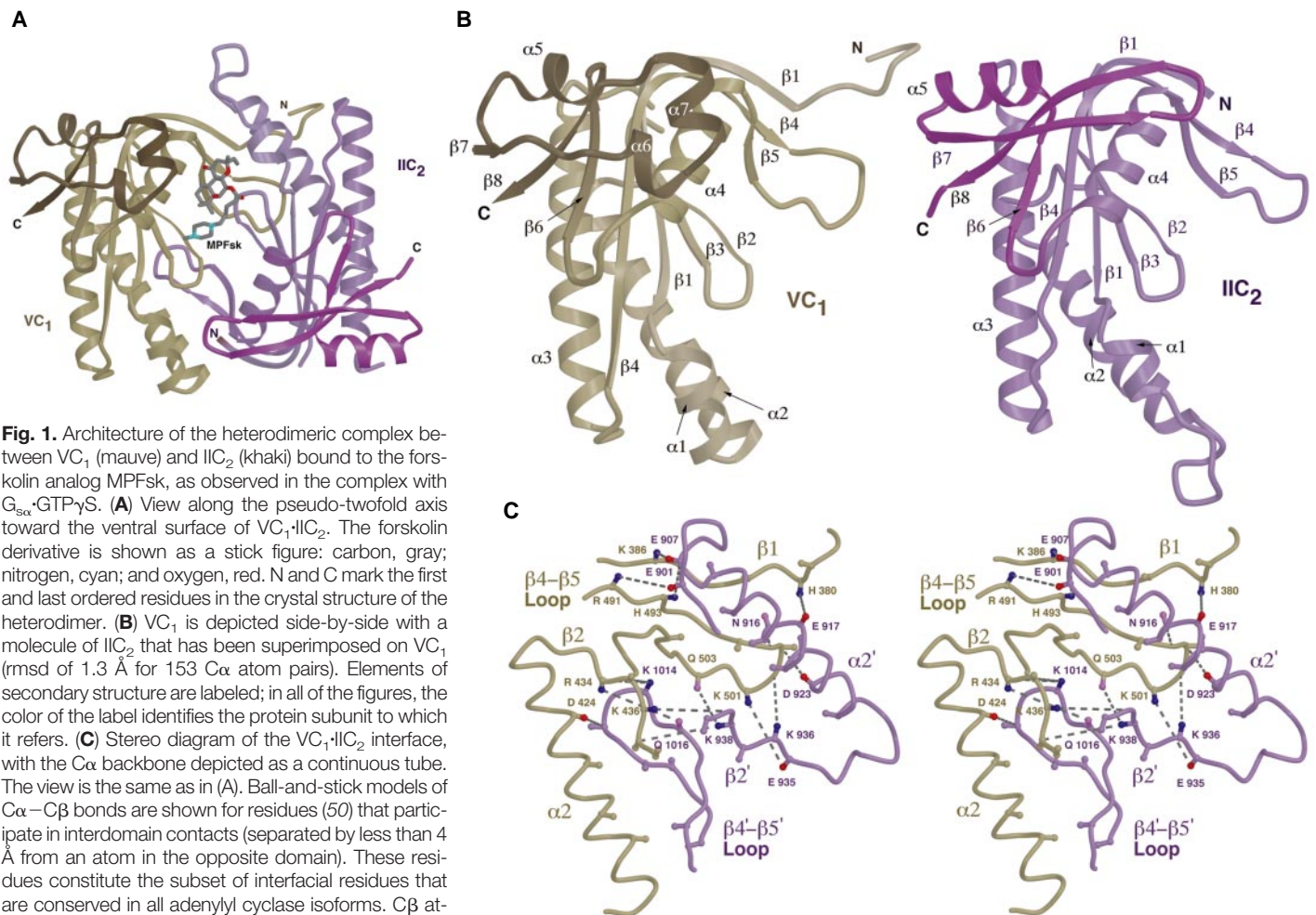


Fig. 1. Architecture of the heterodimeric complex between VC₁ (mauve) and IIC₂ (khaki) bound to the forskolin analog MPFsk, as observed in the complex with G_{s α} -GTP γ S. **(A)** View along the pseudo-twofold axis toward the ventral surface of VC₁-IIC₂. The forskolin derivative is shown as a stick figure: carbon, gray; nitrogen, cyan; and oxygen, red. N and C mark the first and last ordered residues in the crystal structure of the heterodimer. **(B)** VC₁ is depicted side-by-side with a molecule of IIC₂ that has been superimposed on VC₁ (rmsd of 1.3 Å for 153 C α atom pairs). Elements of secondary structure are labeled; in all of the figures, the color of the label identifies the protein subunit to which it refers. **(C)** Stereo diagram of the VC₁-IIC₂ interface, with the C α backbone depicted as a continuous tube. The view is the same as in (A). Ball-and-stick models of C α -C β bonds are shown for residues (50) that participate in interdomain contacts (separated by less than 4 Å from an atom in the opposite domain). These residues constitute the subset of interfacial residues that are conserved in all adenylyl cyclase isoforms. C β atoms of residues with acidic side chains are red, basic residues are blue, and residues with polar side chains are pink. The C β atoms of nonpolar residues are khaki (VC₁) or mauve (IIC₂). Dashed gray lines show interdomain side chain-side chain or side chain-main chain hydrogen bonds

or ion pairs involving polar or charged interfacial residues. Only the polar or charged residues are labeled. Figures were drawn with the program BOB-SCRIPT (51) and rendered with RASTER3D (52).

COOH-terminal end of β_4 , and the α_1 '- α_2 ' loop abuts the β_5 - α_4 turn and the midsections of β_1 and β_4 (Fig. 1B). The interface is composed of both hydrophobic and polar interactions and is further strengthened by the binding of MPFsk between α_1 ' and β_5 (see below). Two of the structural elements

that form this interface, α_1 ' and α_2 ', also form part of the binding site for G_{src} .

The second pseudo-equivalent domain interface, distant from the G_{src} binding site, is significantly different (Fig. 1C). Strand β_2 forms fewer contacts with the β_4 '- β_5 ' loop than does β_2 ' with β_4 - β_5 . The small

number of contacts to the β_2 - β_3 loop, which carries a catalytically essential aspartic acid, may allow this structure to be easily manipulated by regulators of adenylyl cyclase. In addition, the contact of α_2 with IIC_2 is less extensive, and interfacial contacts involving α_1 are essentially absent. Helix α_1 is therefore easily manipulated by the binding of P-site inhibitor and pyrophosphate (see below).

The C_1 · C_2 interface and its asymmetry are crucial to the function of adenylyl cyclase. The interface is responsible for forming the forskolin and G_{src} binding sites at one end and the active site at the other. In addition, we believe that the C_1 and C_2 domains change their relative orientations upon binding of G_{src} , representing, at least in part, a mechanism for activation of adenylyl cyclase by the G protein. Critical to this conformational change is the maintenance of the C_1 · C_2 interfacial contacts in both the unactivated and activated states of the enzyme. As will be discussed below, the C_1 · C_2 interface is formed by flexible elements of one domain (for example, the β_4 '- β_5 ' loop) that interact with elements from the structural core of the other (for example, α_2). Mutations of interfacial residues further highlight the importance of the C_1 · C_2 interface (Table 2). For example, alanine mutants of interfacial residues equivalent to either Asp⁴²⁴ in VC_1 or its counterpart in IIC_2 , Asp⁹²³, are largely inactivating.

Forskolin binding. In contrast to the pair of forskolin molecules bound to the IIC_2 homodimer (14), only one molecule of MPFsk binds to the VC_1 · IIC_2 heterodimer (Figs. 1A and 3). The single forskolin binding site, flanked on one side by β_5 - α_4 and on the other by α_1 ' and the β_2 '- β_3 ' loop, is structurally equivalent to and can be superimposed with both sites in the IIC_2 homodimer (Fig. 3). The forskolin binding site in VC_1 · IIC_2 is adjacent to that for G_{src} . Contacts between forskolin and IIC_2 are generally the same as observed in the IIC_2 homodimer (Lys⁸⁹⁶, Ile⁹⁴⁰, Gly⁹⁴¹, and Ser⁹⁴²). Most of the contacts between forskolin and VC_1 are either identical (Phe³⁹⁴ versus Phe⁸⁸⁹, Trp⁵⁰⁷ versus Trp¹⁰²⁰, Val⁵¹¹ versus Val¹⁰²⁴) or analogous (Tyr⁴⁴³ versus Met⁹⁴⁵) to those between forskolin and the corresponding IIC_2 subunit of the homodimer (Fig. 3). A water molecule bridges the O1 and O4 oxygens of the forskolin analog and the side chain of Ser⁹⁴². The piperazino tail of the forskolin analog used in this study is poorly ordered compared with the remainder of the molecule. However, its proximity to the side chains of Cys⁴⁴¹ and Asn⁵¹⁵ may allow the design of similar extensions that would create an analog with higher affinity.

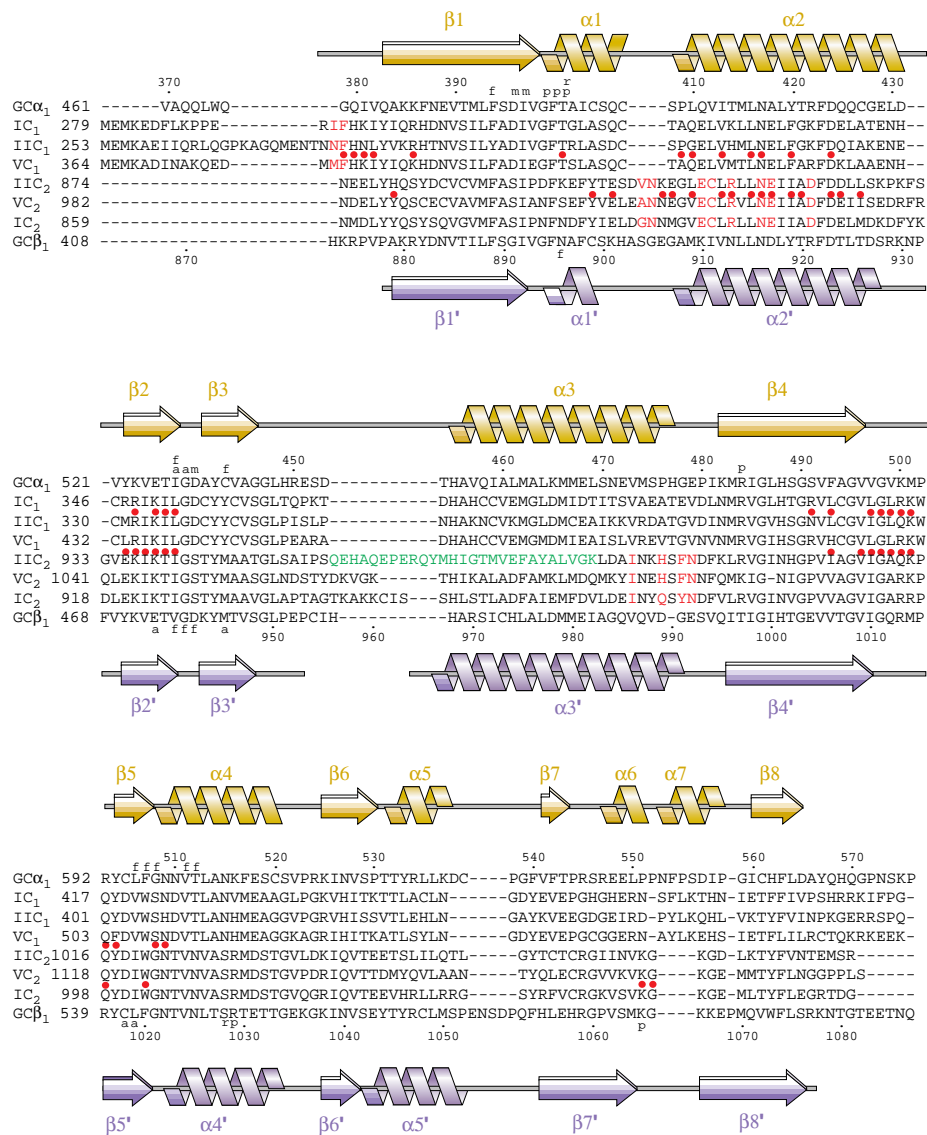


Fig. 2. Structure-based alignment of the amino acid sequences (50) of selected adenylyl and guanylyl cyclase C_1 and C_2 domains. Only the sequences that correspond to the VC_1 and IIC_2 constructs used in this study are shown. $GC\alpha_1$ and $GC\beta_1$ correspond to the α and β subunits of rat soluble guanylyl cyclase (53). The remaining sequences correspond to the C_1 and C_2 domains of various isoforms of adenylyl cyclase, as indicated (4, 54, 55). The top four sequences correspond to C_1 domains, and the lower four correspond to C_2 domains. The amino acid position of each enzyme is shown at the beginning of each line, and the residue numbers for VC_1 and IIC_2 are indicated above and below the alignment, respectively. The secondary structure of the C_1 domain is drawn in khaki above the alignment, and that of the C_2 domain is drawn in mauve below the alignment. Arrows represent β strands, and coils represent α helices. Other secondary structural elements, such as random coils and turns, are represented by a solid line. Disordered regions are indicated by the lack of corresponding secondary structure. Red dots above the sequence of VC_1 or below the sequence of IIC_2 indicate residues from each domain that form the VC_1 · IIC_2 interface. Red amino acid symbols correspond to residues that directly interact with G_{src} . Green amino acid residues indicate the region believed to be important for interactions with the $\beta\gamma$ subunit in IIC_2 (21). Various functional residues in VC_1 and IIC_2 are indicated by symbols: f, forskolin binding; a, adenine binding; p, pyrophosphate binding; m, magnesium binding; and r, ribose binding.

Forskolin cannot bind to the second, pseudosymmetric site of $VC_1 \cdot IIC_2$ (12). Of the residues that would contact the putative forskolin molecule at this site, there are only two that are significantly different from the first site. The Thr⁵¹² residue is replaced by Asn¹⁰²⁵ and, perhaps more importantly, Ser⁹⁴² is replaced by Asp⁴⁴⁰. Both substitutions would result in steric conflicts with a bound molecule of forskolin. As was mentioned above, the relative orientation of the C_1 and C_2 domains within the $G_{s\alpha} \cdot VC_1 \cdot IIC_2$ complex is significantly different from that of the C_2 domains in the IIC_2 homodimer. One effect of this quaternary change is to alter the position of the $\alpha 4'$ helix in the ventral cleft such that the Asn¹⁰²⁵ side chain overlaps the potential forskolin binding site. If the VC_1 domain is superimposed on one of the IIC_2 domains in the homodimer, only the overlap with Asn¹⁰²⁵ is alleviated; that with Asp⁴⁴⁰ is not. Furthermore, the binding of a second molecule of forskolin at this site would inhibit adenylyl cyclase by interfering with substrate binding. Thus, it is very unlikely that two molecules of forskolin bind to the ventral cleft of intact adenylyl cyclase.

When bound to the domain interface, forskolin stabilizes the interaction between VC_1 and IIC_2 (14). Accordingly, forskolin, like $G_{s\alpha}$, increases the apparent affinity of VC_1 for IIC_2 from ≥ 10 to $\sim 1 \mu M$ (11). It

has thus been proposed that forskolin activates adenylyl cyclase by promoting $C_1 \cdot C_2$ association, resulting in formation of an

active site (14). However, forskolin does not significantly affect the inhibition constant (K_i) for the substrate inhibitor

Table 2. Structure-function correlations of various adenylyl cyclase mutants. Mutations made in different isoforms of adenylyl cyclase (first column) are mapped onto VC_1 or IIC_2 (second column). [Mutation name specifies the residue at the given position, mutated to the residue listed at the end (50).] Their observed phenotype is described in the third and fourth columns, and their role in the $VC_1 \cdot IIC_2 \cdot G_{s\alpha}$ complex is described in the fifth column. EC_{50} , median effective concentration; IC_{50} , median inhibitory concentration.

Mutation (isoform)	Context (VC_1 or IIC_2)	$V_{max}^{Fsk^{*+}} / V_{max}^{G_{s\alpha}^{*+}} / G_{s\alpha}^{*+} / \% \text{ bound} \ddagger$	$EC_{50} G_{s\alpha}^{*+} / IC_{50} P\text{-site} \S / K_m ATP^*$	Structural correlate	Ref.
Wild type		++++/+++	+++/+++		
F293A (ACI)	F379 (VC_1)	+++/ND	-/ND/ND	Interacts with $G_{s\alpha}$; $C_1 \cdot C_2$ interface	(27)
D338A (ACI)	D424 (VC_1)	-/+/+	NC/ND/ND	Protein fold; $C_1 \cdot C_2$ interface	(10)
R348A (ACI)	R343 (VC_1)	++++/+++	+++/+++	Salt bridge to D424	(10)
K350A (ACI)	K436 (VC_1)	++++/+++	+++/+++	$C_1 \cdot C_2$ interface	(10)
D354A (ACI)	D440 (VC_1)	-/-/+	NC/ND/ND	Coordinates Mg^{2+} ; potential base	(10)
R398A (ACI)	R484 (VC_1)	+/-/+++	NC/+/+++	Binds Py of pyrophosphate	(10)
H402A (ACI)	H488 (VC_1)	-/-/-	NC/ND/ND	Protein fold	(10)
D419A (ACI)	D505 (VC_1)	-/-/++	NC/ND/ND	Salt bridge to K436	(10)
E432A (ACI)	E518 (VC_1)	+++/+++	NC/+/+	Salt bridge to R484	(10,12)
E518A (VC_1)	Same	+++/-/ND	-/ND/ND	Interacts/supports contacts with $G_{s\alpha}$ in $\alpha 2$ helix; $C_1 \cdot C_2$ interface	(27)
R913A, L914A, N916A, E917A, D921A (IIC_2)	Same	+++/-/ND	-/ND/ND	Interacts/supports contacts with $G_{s\alpha}$ in $\alpha 2$ helix; $C_1 \cdot C_2$ interface	(27)
D908A (ACI)	D923 (IIC_2)	-/-/-	NC/ND/ND	Protein fold; $C_1 \cdot C_2$ interface	(10)
K921A (ACI)	K936 (IIC_2)	+++/+++	NC/+/+++	Salt bridge to D923; $C_1 \cdot C_2$ interface	(10)
K923A (ACI)	K938 (IIC_2)	+++/+++	NC/-/+	Binds adenine N1; $C_1 \cdot C_2$ interface	(10)
H950A (ACI)	H968 (IIC_2)	-/-/+	NC/ND/ND	Protein fold; strained side chain	(10)
N987A, H989A, F991A, N992A (IIC_2)	Same	+++/-/ND	++/ND/ND	Interacts/supports contacts with $G_{s\alpha}$ in $\alpha 3$ helix	(27)
R979A (ACI)	R997 (IIC_2)	-/-/-	NC/ND/ND	Protein fold; salt bridge to D1031	(10)
Y999A (ACI)	Y1017 (IIC_2)	-/-/+	NC/ND/ND	Protein fold	(10)
D1000A (ACI)	D1018 (IIC_2)	-/-/+	NC/ND/ND	Binds adenine N6	(10)
N1025A (IIC_2)	Same	-/-/ND	ND/ND/ND	Active site structure; water coordination	(33)
R1029A (IIC_2)	R1029 (IIC_2)	-/-/++	NC/-/++	Stabilizes transition state; binds P β of pyrophosphate in P-site inhibited complex	(10,33)
R1011A (ACI)	Same	-/-/++	NC/-/++	Stabilizes transition state; binds P β of pyrophosphate in P-site inhibited complex	(10,33)
Y1054A (IIC_2)	Same	ND/-/ND	ND/ND/+	Protein fold	(12)
R1059A (IIC_2)	Same	ND/+/+ND	ND/ND/+	Protein fold	(12)
K1065A (IIC_2)	Same	ND/-/ND	ND/ND/+	Binds Py of pyrophosphate	(12)
K1049A (ACI)	K1067 (IIC_2)	++++/+++	+++/+/+++	Binds N1022 in P-site complex	(10)

*Symbols: (++) , wild-type value; (+) , 2- to 10-fold decrease in activity or K_m ; (-) , ≥ 10 -fold decrease or inactive; ND, not determined; NC, not calculated because affinity was too weak or negligible activity. Activities correspond to those measured with Mg^{2+} as the metal ion. †ACI forskolin-stimulated activity was measured with Mn^{2+} as the metal ion. ‡Symbols: (++) , $\geq 50\%$ of wild-type binding; (+) , 20 to 50% of wild-type binding; (-) , $\leq 20\%$ of wild-type binding or no detectable binding. §Symbols: (++) , wild-type K_i ; (+) , 5- to 100-fold increase in K_i ; (-) , > 100 -fold increase in K_i . ||Activity is dependent on Mn^{2+} .

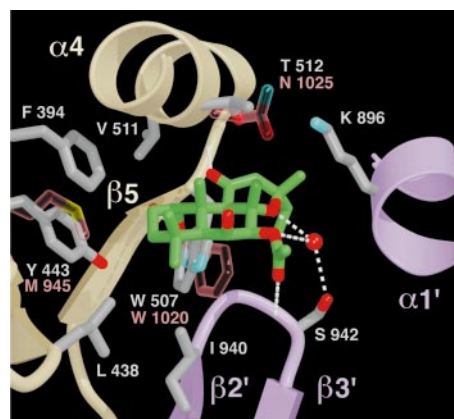


Fig. 3. Only one molecule of forskolin binds in the ventral cleft of $VC_1 \cdot IIC_2$. MPFsk binds in the ventral cleft of adenylyl cyclase at the end closest to the $G_{s\alpha}$ binding site and is drawn in green without its methyl-piperazino group for clarity. Residues constituting the forskolin binding site of the IIC_2 homodimer (14) that differ from their equivalents in the binding site of $VC_1 \cdot IIC_2$ are drawn in transparent rose (50). The side chain of Trp¹⁰²⁰ is also shown because its side chain adopts a dramatically different conformation from that of Trp⁵⁰⁷ in the $VC_1 \cdot IIC_2$ heterodimer. To generate this figure, we superimposed one of the forskolin molecules from the IIC_2 homodimer with MPFsk; this superposition does not optimally align the protein subunits of each structure.

Ap(CH₂)pp nor the Michaelis constant (K_m) of ATP in either our soluble system (12) or for a IC₁-IIC₂ chimera (6, 7). Rather, forskolin increases catalytic activity (V_{max}) by a factor of 60, a factor 10 times greater than its effect on domain association (11). Domain association is obviously a prerequisite for adenylyl cyclase activity. However, domain association alone is clearly not sufficient to achieve the high levels of adenylyl cyclase activity displayed in the presence of forskolin, G_{sα}, or both activators (11). Hence, it is likely that the binding of forskolin facilitates cAMP synthesis by directly altering the conformation of the active site. The structure suggests one way such activation could occur. The β2'-β3' loop contacts Lys⁴³⁶ and Leu⁴³⁸ of the β2-β3 loop of VC₁ (Fig. 1C), thereby linking residues that form the forskolin binding site with structural elements carrying residues important for catalysis (see below).

Interaction of G_{sα} with VC₁·IIC₂. The orientation of G_{sα} relative to VC₁·IIC₂ also suggests that the dorsal surface of the heterodimer is close to the plasma membrane. Thus, substrates would have direct access to the active site of adenylyl cyclase from the cytoplasm, and the palmitoylated NH₂-terminus of native G_{sα} would be close to the membrane (Fig. 4). The orientation, as proposed here, of the α subunit with respect to the mem-

brane is the same as that suggested for the α subunit in the heterotrimer and in models of the receptor complex (25, 26).

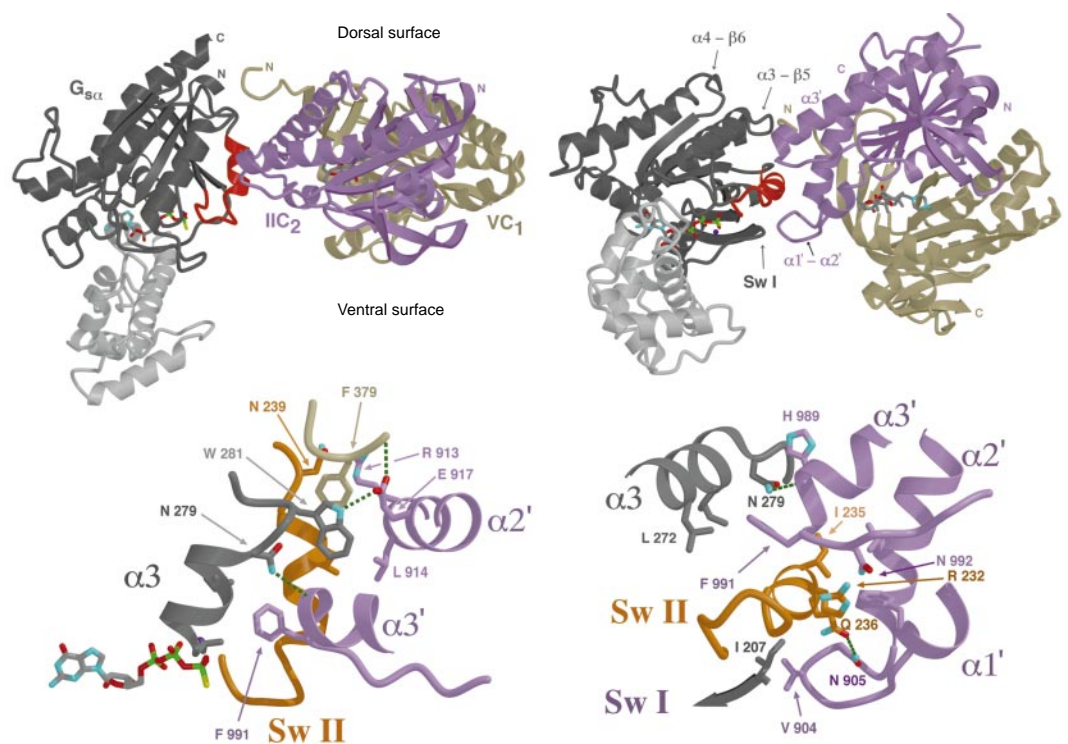
The interface between G_{sα} and VC₁·IIC₂ buries 1800 Å² of solvent-accessible surface area. Two structural elements of G_{sα} form the interface, primarily through contacts with IIC₂ (Fig. 4). The most striking interaction is the insertion of the G_{sα} switch II helix (residues 225 to 240) into the groove formed by α2' and the α3'-β4' loop of adenylyl cyclase. Yan *et al.* (27) correctly identified this G_{sα} binding surface of adenylyl cyclase by mutagenic analysis of the recombinant enzyme. The second contact surface is formed by the α3-β5 loop of G_{sα}, which interacts with both VC₁ and IIC₂. These two adenylyl cyclase-interacting surfaces on G_{sα} were identified by the scanning mutagenesis performed by Berlot and Bourne (28) and (for the α3-β5 loop) by Itoh and Gilman (29). In contrast, the α4-β6 loop of G_{sα}, which was also predicted to interact with adenylyl cyclase (28), is located more than 10 Å from the interface and does not interact with VC₁·IIC₂. Although it is difficult for us to imagine how the α4-β6 loop of G_{sα} could interact with adenylyl cyclase, we cannot exclude the possibility that this loop interacts with elements of adenylyl cyclase that are not present in our constructs.

All of the residues that interact with G_{sα}

are conserved among adenylyl cyclase isoforms (Fig. 2). The G_{sα}·IIC₂ interface is a mixture of hydrophobic and polar contacts, whereas G_{sα}·VC₁ contacts are entirely hydrophobic (Fig. 4). Only two of the G_{sα} residues involved in these interfaces with adenylyl cyclase, Gln²³⁶ and Asn²³⁹, are significantly different from analogous residues (His²¹³ and Glu²¹⁷) in the inhibitory G protein α subunit, G_{iα}. However, these substitutions are conservative with respect to the structure of the interface with adenylyl cyclase. Therefore, the specificity of G_{sα} and G_{iα} subunits for adenylyl cyclase appears to be dictated primarily by the backbone conformation of the residues that form the interface, not their primary structure (15).

The regions of G_{iα} that interact with adenylyl cyclase have recently been determined by scanning mutagenesis; they map to switch II and, less convincingly, to the α4-β6 loop, but not to the α3-β5 loop (30). Furthermore, inhibition of ACV and ACVI is not competitive with respect to G_{sα} (31). Therefore, G_{iα} appears to bind a site on adenylyl cyclase distinct from that of G_{sα}. Given the homology of G_{sα} and G_{iα} and their presumably similar orientation with respect to the membrane, the most attractive binding site for G_{iα} is between the α1-α2 loop and the α3 helix on VC₁, directly opposite to the binding site of G_{sα}.

Fig. 4. The complex between G_{sα}·GTPγS and VC₁·IIC₂ (50). The top of the figure shows two views of the complex. At top left, the complex is drawn with the wide, interdomain cleft (ventral surface) between the C₁ and C₂ domains facing the bottom of the page. The dorsal surface, which is presumed to face the plasma membrane, faces upward. The two adenylyl cyclase domains are colored as in Fig. 1; the ras-like domain of G_{sα} is colored charcoal, and the helical domain is ash gray. The switch II segment (Sw II) (which includes the α2 helix of G_{sα}) is red. GTPγS and MPFsk are depicted as stick figures with the atomic coloring scheme used in Fig. 1. At bottom left is a detail of the G_{sα}·VC₁·IIC₂ interface in about the same orientation as that directly above. Hydrogen bonds are depicted with dashed green lines. Side chain carbon atoms are colored according to the main chain to which they are attached. Of note is the intimate cluster formed by the NH₂-terminus of VC₁, α2' of IIC₂, and both switch II and the α3 helix of G_{sα}. The GTPγS bound to G_{sα} is shown for reference. At top right, the view of the complex is related by a rotation of ~70° about a horizontal axis relative to the view shown on the top left. This rotation



brings the helical domain of G_{sα} toward the reader and provides a view of the ventral surface of VC₁·IIC₂. At bottom right is a detailed view of the interface in the same orientation as that shown directly above.

This region contains many residues that are invariant in ACV and ACVI (for example, Glu³⁹⁸ and Leu⁴⁷²) but not in $G_{s\alpha}$ -insensitive cyclases. The binding of $G_{s\alpha}$ at this site could easily influence the structure of the active site and cause inhibition.

Many mutations inhibit activation of adenylyl cyclase by $G_{s\alpha}$ (Table 2). Several of these involve the residues that constitute the $G_{s\alpha}$ binding site; more interesting are those that do not interfere with either $G_{s\alpha}$ binding or the fold of the protein. Certain mutations, such as those that correspond to Asp⁹²³ and Lys⁹³⁶, are involved in maintenance of the $C_1 \cdot C_2$ interface (Fig. 1C). Although $G_{s\alpha}$ still binds to these mutants, its apparent affinity is less, presumably because the α subunit is unable to effect the proper conformational change at the $C_1 \cdot C_2$ interface. Other mutants, such as Asp⁴⁴⁰ or Arg¹⁰²⁹, are intimately involved in active site structure and catalysis and therefore have greatly inhibited activity.

Binding of P-site inhibitors. P-site analogs act as dead-end inhibitors of pyrophosphate (product) release and inhibit adenylyl cyclase only in the presence of pyrophosphate and Mg^{2+} or Mn^{2+} (32). Although these compounds are noncompetitive or uncompetitive inhibitors of cAMP synthesis, they are competitive with cAMP in the reverse reaction (32). Furthermore, kinetic studies of P-site inhibition and the structure of the complex itself both strongly suggest that the P-site and the substrate (ATP) binding site are the same. The P-site inhibitor-pyrophosphate- Mg^{2+} complex therefore best mimics the product complex of adenylyl cyclase (Fig. 5A).

Pyrophosphate, 2',d3'-AMP, and Mg^{2+} bind to the end of the ventral cleft of $VC_1 \cdot IIC_2$ that is farthest from $G_{s\alpha}$. The three ligands are not well ordered in the structure and exhibit high-temperature factors, suggesting incomplete occupancy or incomplete formation of the binding pocket due to constraints imposed by the crystalline lattice. However, omit maps clearly demonstrate where each molecule binds (Fig. 5B). The site is pseudosymmetric to the binding site for forskolin. Similarly, the P-site is formed by $\alpha 1$ and its preceding loop, the $\beta 2$ - $\beta 3$ loop, $\beta 4$, and $\beta 4'$ - $\alpha 4'$. Pyrophosphate is positioned over a P-loop at the NH_2 -terminus of $\alpha 1$ and is bound by Mg^{2+} and three basic residues: Arg⁴⁸⁴ ($\beta 4$), Arg¹⁰²⁹ ($\alpha 4'$), and Lys¹⁰⁶⁵ ($\beta 7'$ - $\beta 8'$ turn). Three periplanar ligands of the Mg^{2+} ion are formed by Asp³⁹⁶ ($\beta 1$), Asp⁴⁴⁰ ($\beta 2$ - $\beta 3$ loop), and an oxygen atom from the β phosphate of pyrophosphate. One axial ligand is donated by the carbonyl oxygen of residue 397. The unoccupied coordination sites of Mg^{2+} could easily be filled by water molecules, although none are apparent in our structure. In the native structure of the $G_{s\alpha} \cdot VC_1 \cdot IIC_2$ complex, weak electron density, presumably that of Mg^{2+} , also occurs between the side chains of Asp³⁹⁶, Asp⁴⁴⁰, and the carbonyl oxygen of residue 397.

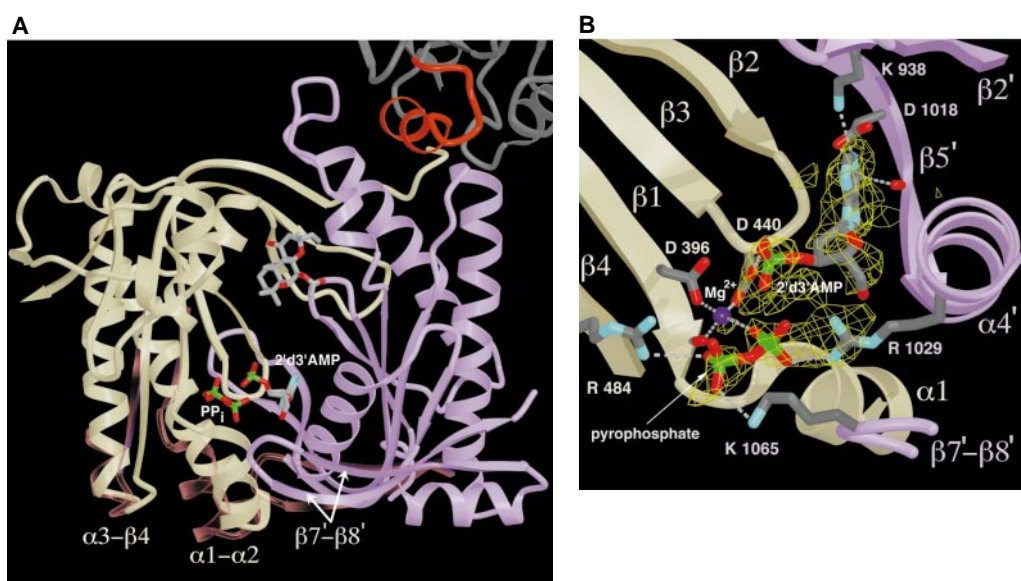
The purine ring is stacked over the peptide plane of residues 438 and 439. Adenine nucleotides are recognized, to the exclusion of guanine, by hydrogen bonds from the purine N6 atom to Asp¹⁰¹⁸ ($\beta 5'$) and the backbone carbonyl of resi-

due 1019. A hydrogen bond is also formed between Lys⁹³⁸ ($\beta 2'$) and the purine N1 atom. In the guanylyl cyclases, the residues corresponding to Asp¹⁰¹⁸ and Lys⁹³⁸ are substituted by cysteine and glutamate (Fig. 2), respectively, perhaps explaining the difference in specificity for purine nucleotides. The alanine mutant in ACI of the residue corresponding to Asp¹⁰¹⁸ in IIC_2 is inactivating (Table 2).

The ribosyl moiety of 2',d3'-AMP appears to adopt a 2'-endo conformation, with its O4' atom packing against the side chain of Ser¹⁰²⁸ ($\alpha 4'$) and its 5'-hydroxyl forming a hydrogen bond with the side chain of Thr⁴⁰¹. The purine ring is *anti* to the ribose ring. The 3'-phosphate P α -O3' bond is *trans* to the ribose C3'-C4' bond, and the 3'-phosphate binds between the P β of pyrophosphate and Asp⁴⁴⁰, perhaps forming hydrogen bonds to each. The complex formed with 2',d3'-ATP is essentially identical to that formed with 2',d3'-AMP; the two additional phosphate groups appear disordered. Potential interactions with positively charged residues surrounding the opening of the catalytic site may account for the increase by a factor of 10 in the apparent affinity for adenylyl cyclase (13) afforded by the 3'-triphosphate group.

The most potent P-site inhibitors have 3' mono or polyphosphates, and 2',5'-dideoxyribose moieties. In the conformation of the nucleotide bound to adenylyl cyclase, the 3'-phosphate appears to form hydrogen bonds with both Asp⁴⁴⁰ and pyrophosphate. A 2'-hydroxyl, which is absent in 2',d3'-AMP, would collide with the 3'-phosphate.

Fig. 5. Global and detailed views of the complex between the P-site inhibitor 2',d3'-AMP, pyrophosphate, and $VC_1 \cdot IIC_2$. The view is toward the ventral face of $VC_1 \cdot IIC_2$. (A) The P-site inhibitor and pyrophosphate are bound in the ventral cleft at the end furthest from $G_{s\alpha}$ (the switch II region of $G_{s\alpha}$ is red and its surrounding structural elements are charcoal) (50). The P-site is related by a pseudo-twofold axis of symmetry to the MPFsk binding site. MPFsk is modeled as a molecule of forskolin because its methylpiperazino tail was very poorly ordered in the P-site-inhibited structure. The position of the $\beta 1$ - $\alpha 1$ - $\alpha 2$ and $\alpha 3$ - $\beta 4$ elements of VC_1 and the $\beta 7'$ - $\beta 8'$ β ribbon of IIC_2 in the absence of P-site inhibitor and pyrophosphate are depicted as transparent, rose-colored ribbons. (B) Detail of the catalytic site showing 2',d3'-AMP, pyrophosphate, and Mg^{2+} (purple). The green wire cage depicts $F_o - F_c$ difference electron density contoured at the 2.0σ level. Crystallographic phases used in the calculation of this map were based on an atomic coordinate set obtained after modeling and refinement of the conformational changes described



above, but before inclusion of coordinates for 2',d3'-AMP, pyrophosphate, and Mg^{2+} (see legend to Table 1 for experimental details). Hydrogen bonds and coordination to Mg^{2+} are depicted with gray dashed lines.

The 5'-hydroxyl of 2',d3'-AMP is not well ordered, and its removal may permit a 5'-deoxy P-site inhibitor to bind in a slightly different orientation that has more favorable interactions with the protein.

Diffusion of P-site inhibitors into crystals of the $G_{s\alpha}\cdot VC_1\cdot IIC_2\cdot MPFsk$ complex is accompanied by segmental conformational changes in VC_1 and IIC_2 (Fig. 5A). The most prominent of these is the rotation of

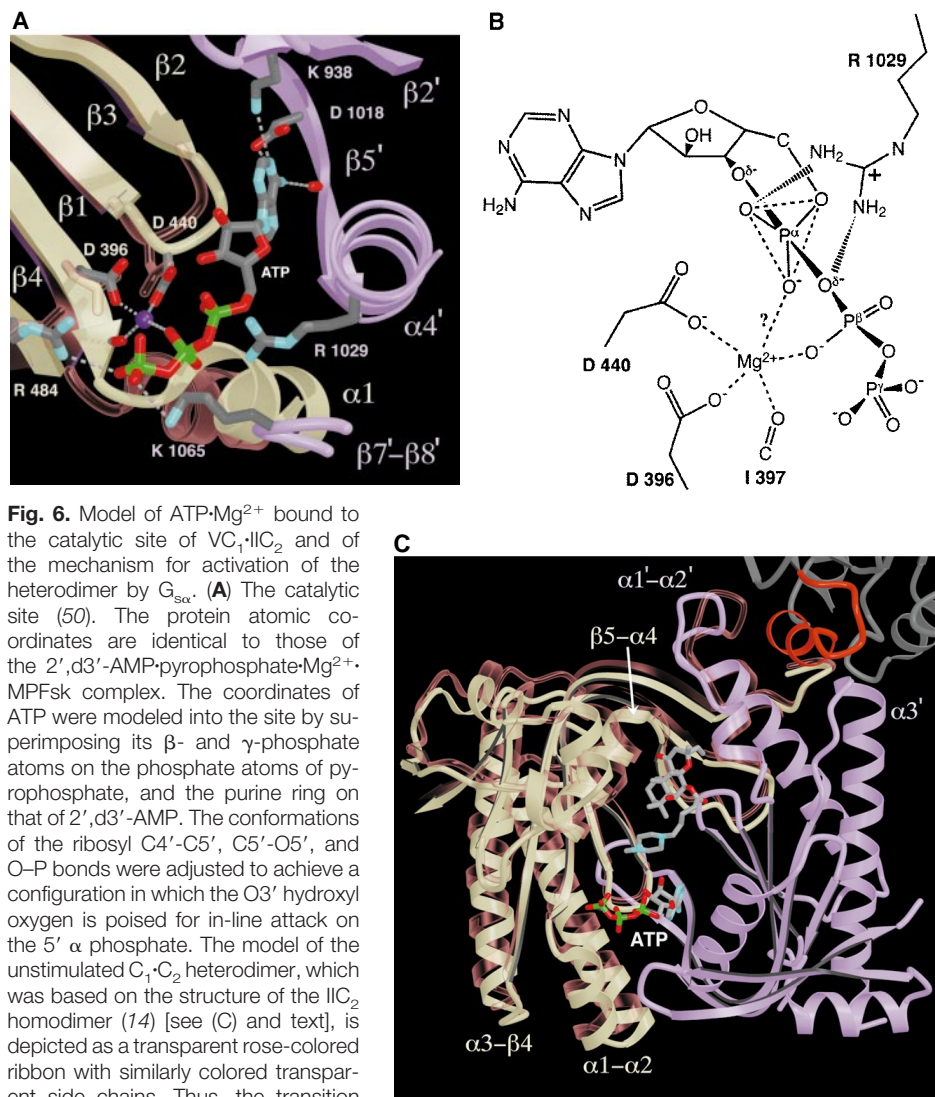
$\alpha 1$ and the adjacent $\alpha 3$ - $\beta 4$ loop of VC_1 toward the pyrophosphate binding site. The $\alpha 1$ helix forms new contacts with the $\alpha 4'$ helix of IIC_2 , most notably to Asn¹⁰²⁵, a residue implicated in the catalytic mechanism of adenylyl cyclase (33). We suspect the $\alpha 1$ helix behaves like a lid for the active site that closes upon ligand binding. The $\beta 7'$ - $\beta 8'$ β ribbon swings over the P-site, where Lys¹⁰⁶⁵ forms an ion pair

with pyrophosphate.

In general, mutations that affect the K_i 's for P-site inhibition affect the K_m 's for ATP to a lesser extent (Table 2). For example, the alanine mutant of the residue equivalent to Lys⁹³⁸ is only partially inactivating, but it increases the K_i of 2',d3'-AMP by a factor of 250 compared with a factor of 3 increase in the K_m of ATP (10). These phenomena are consistent with the fact that P-site inhibitors bind most tightly to the $G_{s\alpha}$ - and forskolin-activated, pyrophosphate-bound complex of adenylyl cyclase (28). We suspect that the conformation of the ATP-bound enzyme differs from that of the 2',d3'-AMP-pyrophosphate complex described here. Catalysis may require a conformational transition subsequent to ATP binding, resulting in a cAMP-bound conformation similar to that observed here in the presence of 2',d3'-AMP. Such a transition would potentially involve residues such as Lys⁹³⁸ that form the C_1 - C_2 interface. Thus, mutation of interfacial residues, which may hinder the conformational changes required for catalysis, necessarily reduces P-site binding to a much greater extent than ATP binding. From a kinetic rather than a structural point of view, any mutation that slows catalysis will impair accumulation of the enzyme-pyrophosphate complex, which is essential for observation of P-site inhibition (32).

Adenylyl cyclase catalytic mechanism. Analysis of the stereochemistry of the cyclase-catalyzed reaction, using diastereomers of adenosine-5'-(α -thio)triphosphate (ATP α S) or the corresponding guanine nucleotide, demonstrated that cyclization proceeds with an inversion of configuration at the α phosphate (34-37). A direct, in-line attack of the O3' hydroxyl on the 5' α phosphate, without formation of a phospho-enzyme intermediate, most easily accounts for these results. To catalyze this reaction, the enzyme might be expected to provide a base to deprotonate the 3'-hydroxyl of ATP and a cationic residue or metal to stabilize a pentavalent phosphate intermediate.

From the above discussions, it is obvious that the binding site for ATP is formed by both domains and that the individually expressed cytosolic domains are unlikely to be catalytic, despite claims to the contrary (14, 38). A model of ATP bound to the active site can be constructed (Fig. 6A) in which the position of pyrophosphate-Mg²⁺ and a purine ring in the P-site complex is presumed to approximate that of the β and γ phosphates and the adenine of ATP. The conformation adopted by the α phosphate would allow in-line attack by the 3' oxyanion with



pyrophosphate as the leaving group. The Mg^{2+} coordination sphere would be similar to that observed in the P-site complex, with possible interaction of the α phosphate with Mg^{2+} in the transition state.

The Arg¹⁰²⁹ residue ($\alpha 4'$) is essential for catalytic activity (Table 2) and is poised to stabilize the pentacoordinate α phosphate intermediate of the reaction (Fig. 6B). This arginine may also stabilize the growing charge on the leaving β phosphate of pyrophosphate. However, mutation of Arg¹⁰²⁹ does not perturb the K_m for ATP (Table 2). Thus, Arg¹⁰²⁹ is exactly analogous to Arg¹⁷⁸ of $G_{\alpha 1}$ and Arg²⁰¹ of $G_{\alpha 2}$, which stabilize the transition state of GTP hydrolysis in α subunits (19, 39), yet do not interact with GTP in the ground state (15, 19). The Arg¹⁰²⁹ residue is, however, very important for P-site inhibition (Table 2) and directly binds pyrophosphate in the inhibited complex. The invariant Asn¹⁰²⁵, which also appears to be essential for the catalytic mechanism (Table 2), seems important for the conformational change that occurs upon ligand binding ($\alpha 1$ helix contact) and may help bind ATP by coordinating a water molecule that forms a hydrogen bond with the N9 atom of ATP.

Our structures do not clearly indicate how the 3'-hydroxyl is deprotonated. The side chain of Asp⁴⁴⁰ is close to the ribose 3'-hydroxyl group and is therefore a potential catalytic base, although the basicity of this residue is presumably very low because of its participation in the ligand field of Mg^{2+} . It is also feasible that the α phosphate serves as the general base; similar substrate-assisted mechanisms have been suggested for glutaminyl tRNA synthetase (40) and for p21^{ras} (41). The environment in the vicinity of the ribose 3'-hydroxyl group is highly electronegative, with the preponderance of negative charges arising from Asp⁴⁴⁰, Asp³⁹⁶, and the α phosphate of the nucleotide. These groups would actually increase the pK_a (where K_a is the acid constant) of the 3'-hydroxyl, hindering deprotonation. Perhaps a second metal ion, not identified in the present study, binds to the ATP complex and polarizes the 3'-hydroxyl. The conformation of bound ATP, the active site, or both may also be significantly different than suggested by our model. This idea is supported by the fact that we failed to observe binding of Ap(CH₂)pp in soaking experiments similar to those used for the P-site inhibitor.

It has been pointed out that the $\beta\alpha\beta\beta\alpha\beta$ fold of adenylyl cyclase bears remarkable similarity to the catalytic scaffold of the DNA polymerase I palm domain (42). The chemical transformation catalyzed by each enzyme is also similar:

intra- (cyclase) compared with inter- (polymerase) molecular attack of a 3'-hydroxyl on a 5'-phosphate. The resemblance between these two enzyme families extends to the position of two (cyclase) out of typically three (polymerase) acidic residues that are responsible for coordinating metal ions in the polymerases (43). The polymerases are proposed to bind two metal ions at the site of primer extension, whereas only one is observed in our P-site-inhibited complex. The proposed role of the first metal ion is to polarize the 3'-hydroxyl and stabilize the pentavalent intermediate. The role of the second ion is likewise to stabilize the transition state and to bind the polyphosphate tail of the nucleotide. In our structure, the observed magnesium ion is analogous to the second polymerase metal site. The role of the first metal ion could be partially assumed by the invariant Arg¹⁰²⁹, which may stabilize the pentavalent phosphate transition state.

Our comments regarding the mechanism of the adenylyl cyclase-catalyzed reaction are speculative. The resolution to which the structure of the P-site complex is currently determined is not sufficient to define the position of potential catalytic residues with great precision. Further, we cannot rule out the possibility that additional metal ions remain undetected in the structure. Our failure, so far, to diffuse Ap(CH₂)pp into crystals of $G_{\alpha 2}\cdot VC_1\cdot IIC_2$ may be indicative of potential conformational changes that accompany substrate binding. Thus, the P-site analog, presumably a good mimic of cAMP, may be a poor analog of ATP. Higher resolution studies of substrate (ATP analogs), product cAMP, and P-site inhibitors are required.

Mechanism of activation by $G_{\alpha 2}$. There are several mechanisms by which $G_{\alpha 2}$ could stimulate adenylyl cyclase. The first of these is to direct productive formation of the $C_1\cdot C_2$ interface, a role that has been suggested for forskolin. However, as discussed with regard to forskolin above, there are a number of observations that suggest that $G_{\alpha 2}$ acts primarily as an allosteric activator of adenylyl cyclase. $G_{\alpha 2}$ interacts with both the C_1 and C_2 domains of adenylyl cyclase. Of the 1800 Å² of surface area buried upon $G_{\alpha 2}$ binding, 75% is with the C_2 domain and 25% is with the C_1 domain. However, $G_{\alpha 2}$ can bind to monomeric IIC_2 alone (disrupting IIC_2 homodimers) (11), demonstrating that C_1 is not required for binding. A C_1 domain with phenylalanine at the position equivalent to 379 of VC_1 is, however, important for activation of adenylyl cyclase (27). Furthermore, given the large surface area buried between C_1 and C_2 , the reasonably

large hydrophobic component of their interface, and the fact that they are covalently linked in the native protein, it seems unlikely that they are ever dissociated in vivo. The binding of $G_{\alpha 2}$ to either the mixture of C_1 and C_2 domains of adenylyl cyclase, or to fusion constructs of these, has little effect on the K_m for ATP or the K_i for Ap(CH₂)pp (6, 7, 12). $G_{\alpha 2}$ and forskolin bind synergistically (11) and thus stabilize the same form of the enzyme. Finally, together and separately, the two activators promote catalysis to a degree that exceeds their effect on domain association, and association of domains per se is an insufficient stimulus to catalysis. Therefore, $G_{\alpha 2}$, like forskolin, appears to activate adenylyl cyclase primarily by stabilizing a catalytically competent form of the enzyme.

We propose that the binding of $G_{\alpha 2}$ to adenylyl cyclase induces a change in the relative orientation of the C_1 and C_2 domains that, in turn, primes the active site for catalysis. Because the structure of the $VC_1\cdot IIC_2$ heterodimer in the absence of bound $G_{\alpha 2}$ has not yet been determined, the conformational mechanism by which $G_{\alpha 2}$ activates adenylyl cyclase is not directly evident. However, the structure of the forskolin-bound C_2 homodimer might approximate that of $VC_1\cdot IIC_2$ in the absence of $G_{\alpha 2}$ and allow us to postulate a mechanism. Several observations support this view. First, the regions of VC_1 that form the interface with IIC_2 superimpose with their counterparts in IIC_2 with a rmsd of 0.9 Å (114 C α atom pairs). Despite the presence of residues that are not conserved between VC_1 and IIC_2 within the interface, superposition of VC_1 on one of the subunits in the IIC_2 homodimer reveals no significant steric or charge conflicts involving these residues. In addition, most of these nonconserved residues are themselves nonconserved in their respective C_1 or C_2 domains of other cyclase isoforms, suggesting that they play only minor roles in interface stabilization.

Comparison of the A subunit of the IIC_2 homodimer with that of IIC_2 in the $VC_1\cdot IIC_2$ heterodimer (difference distance plots) reveals that residues 900 to 913 ($\alpha 1'\text{-}\alpha 2'$ loop), 879 to 883 (NH₂-terminus of $\beta 1'$), and 1005 to 1020 ($\beta 4'\text{-}\beta 5'$) adopt different conformations from the remainder (the core) of the C_2 domain in each structure. Omitting these elements, the two IIC_2 molecules superimpose with a rmsd of 0.4 Å (127 C α atom pairs), as opposed to 0.8 Å for the entire molecule (164 C α atom pairs). Notably, these elements form many interfacial contacts with the analogous structural core of C_1 . The NH₂-terminus and $\beta 4\text{-}\beta 5$ loop of C_1 ,

which form analogous contacts with the core of the C₂ domain, are likewise expected to have conformational flexibility. C₁ and C₂ thus embrace each other in flexible arms that allow the two domains to change their relative orientation, yet remain associated (Fig. 1C).

G_{sa} could induce domain reorientation by inserting its switch II helix into the cleft between the α1'-α2' loop and the α3' helix of IIC₂. This intrusion widens the cleft by 3 Å at the outermost point (Fig. 6C). The α1'-α2' loop rotates away from the core C₂ domain and, through its extensive contacts with the β5-α4 region of the C₁ domain, forces the core of the C₁ domain to rotate by 7° around an axis roughly parallel with the ventral cleft of the heterodimer. This rotation decreases the pseudo-twofold symmetry of the C₁·C₂ heterodimer. The NH₂-terminus of VC₁ is tethered between G_{sa} and IIC₂; thus, this region may provide an anchor that allows G_{sa} to apply torque to the C₁ core domain. In the active site of adenylyl cyclase, the result of this rotation is to move the β2-β3 loop toward and the β4 strand (carrying Arg⁴⁸⁴) away from the core of the C₂ domain (Fig. 6A). Most notable in this activation model is the shift of P-loop residues at the NH₂-terminus of α1 and of the β2-β3 loop relative to elements of the nucleotide binding site in β5' and α4'. This movement would bring Asp⁴⁴⁰ closer to the 3'-hydroxyl group of the substrate. Mutation of the residue equivalent to Arg⁴⁸⁴ in VC₁ eliminates activation by G_{sa}, highlighting the importance of this residue for the mechanism of G_{sa} activation (Table 2). Although this pyrophosphate-binding residue is not expected to be catalytic, its registration with other residues in the active site, in particular Arg¹⁰²⁹ (α4'), may be essential for positioning Arg¹⁰²⁹ to interact with the pentavalent transition state of the substrate (Fig. 6B). In these ways, G_{sa} can improve transition-state stabilization and potentiate a chemical step in the reaction mechanism. The structure of a C₁·C₂ heterodimer in the absence of G_{sa}, along with structures that display the position of substrate analogs, will provide much additional insight into the mechanism of activation of adenylyl cyclase by G protein α subunits.

REFERENCES AND NOTES

1. R. Sunahara, C. Dessauer, A. Gilman, *Annu. Rev. Pharmacol. Toxicol.* **36**, 461 (1996).
2. R. lyengar, *FASEB J.* **7**, 768 (1993).
3. Z. Xia and D. R. Storm, *Curr. Opin. Neurobiol.* **7**, 391 (1997).
4. J. Krupinski, F. Coussen, H. A. Bakalyar, W.-J. Tang, P. G. Feinstein, *Science* **244**, 1558 (1989).
5. M. Chinkers and D. L. Garbers, *Annu. Rev. Biochem.* **60**, 553 (1991).
6. C. W. Dessauer and A. G. Gilman, *J. Biol. Chem.* **271**, 16967 (1996).
7. W.-J. Tang and A. G. Gilman, *Science* **268**, 1769 (1995).
8. R. E. Whisnant, A. G. Gilman, C. W. Dessauer, *Proc. Natl. Acad. Sci. U.S.A.* **93**, 6621 (1996).
9. S.-Z. Yan, D. Hahn, Z.-H. Huang, W.-J. Tang, *J. Biol. Chem.* **271**, 10941 (1996).
10. W.-J. Tang, M. Stanzel, A. G. Gilman, *Biochemistry* **34**, 14563 (1995).
11. R. K. Sunahara, C. W. Dessauer, R. E. Whisnant, C. Kleuss, A. G. Gilman, *J. Biol. Chem.* **272**, 22265 (1997).
12. C. W. Dessauer, T. T. Scully, A. G. Gilman, *ibid.*, p. 22272.
13. L. Desaubry, I. Shoshani, R. A. Johnson, *ibid.* **271**, 2380 (1996).
14. G. Zhang, Y. Liu, A. E. Ruoho, J. H. Hurley, *Nature* **386**, 247 (1997).
15. R. K. Sunahara, J. J. G. Tesmer, A. G. Gilman, S. R. Sprang, *Science* **278**, 1943 (1997).
16. The VC₁·IIC₂·G_{sa}·GTPγS complex was purified by gel filtration, as described (11), in the presence of forskolin. The running buffer contained 20 mM sodium Hepes (pH 8.0), 2 mM MgCl₂, 1 mM EDTA, 2 mM dithiothreitol (DTT), 100 mM NaCl, 25 μM forskolin, and 10 μM GTPγS. After the appropriate fractions were pooled, DTT, MPFsk, and GTPγS were added to final concentrations of 5 mM, 200 μM, and 500 μM, respectively. The complex was concentrated to ~8 mg ml⁻¹ with an Amicon Centricon with a 50-kD cutoff, and the protein was divided into samples and frozen in liquid nitrogen. Crystals of the complex were obtained by vapor diffusion at room temperature in which 4- to 6-μl drops containing concentrated protein mixed 1:1 with well solution were suspended over a 1-ml well containing 7.2 to 7.5% polyethylene glycol (PEG) 8K, 500 mM NaCl, and 100 mM MES (pH 5.4 to 5.6). Crystals appeared as stacks of thin plates within 2 days and grew to their maximum size over a period of 2 weeks. Single crystals of suitable size for data collection, typically 200 μm by 100 μm by 10 μm, were obtained by breaking up the stacks and then soaking them in a harvesting solution containing 100 mM MES (pH 5.4), 9% PEG 8K, 500 mM NaCl, 5 mM MgCl₂, 20 mM sodium Hepes pH 8.0, 1 mM EDTA, 2 mM DTT, 200 μM MPFsk, and 100 μM GTPγS, plus 30% PEG 400 as the cryoprotectant. For the P-site-inhibited complex, crystals were soaked in a harvesting solution that also included either 3.5 mM 2',d3'-AMP plus 3.5 mM pyrophosphate or 100 μM 2',d3'-ATP plus 2 mM pyrophosphate for 2 hours. Other compounds that we attempted to soak into native crystals included 1.4 mM Ap(CH₂)₂pp, 7 mM ATP, and 7 mM 2'-iodo-ATP. The diffraction amplitudes collected from these crystals were not significantly different from those of the native complex, although the ATP-soaked crystals suffered a considerable increase in mosaicity and loss of high-resolution diffraction. The 2'-iodo-ATP data set was actually superior to that of the native data and thus is treated as "native."
17. M. P. Graziano, P. J. Casey, A. G. Gilman, *J. Biol. Chem.* **262**, 11375 (1987).
18. The IIC₂ we used was initially derived by limited proteolysis of a longer COOH-terminal fragment of rat ACII (spanning residues 847 to 1090) by using the protease clostripain (Sigma). The resulting 23-kD fragment, which retained full adenylyl cyclase activity when reconstituted with the C₁ domain from ACI, was purified by Mono Q anion exchange chromatography. The NH₂-terminal proteolysis site and length of this fragment were determined by NH₂-terminal sequencing and mass spectroscopy. Subsequently, a new expression vector (PQE60-ArgC-IIC₂) was created to produce the same C₂ fragment (IIC₂) without a hexahistidine tag. Recombinant IIC₂ was purified from the bacterial lysate by Q-Sepharose anion exchange, followed by filtration through a hydroxyapatite column and then Mono Q and phenyl Sepharose fast protein liquid chromatography steps.
19. D. E. Coleman *et al.*, *Science* **265**, 1405 (1994).
20. A. T. Brünger, *Nature* **355**, 472 (1992).
21. J. Chen *et al.*, *Science* **268**, 1166 (1995).
22. Y. Chen *et al.*, *Proc. Natl. Acad. Sci. U.S.A.* **94**, 2711 (1997).
23. J. F. Leszczynski and G. D. Rose, *Science* **234**, 849 (1986).
24. B. Lee and F. M. Richards, *J. Mol. Biol.* **55**, 379 (1971).
25. D. G. Lambright *et al.*, *Nature* **379**, 311 (1996).
26. O. Lichtarge, H. Bourne, F. Cohen, *Proc. Natl. Acad. Sci. U.S.A.* **93**, 7507 (1996).
27. S.-Z. Yan, Z.-H. Huang, V.-D. Rao, J. H. Hurley, W.-J. Tang, *J. Biol. Chem.* **272**, 18849 (1997).
28. C. H. Berlot and H. R. Bourne, *Cell* **68**, 911 (1992).
29. H. Itoh and A. G. Gilman, *J. Biol. Chem.* **266**, 16226 (1991).
30. G. Grishina and C. H. Berlot, *ibid.* **272**, 20619 (1997).
31. R. Taussig, W.-J. Tang, J. R. Hepler, A. G. Gilman, *ibid.* **269**, 6093 (1994).
32. C. W. Dessauer and A. G. Gilman, *ibid.* **272**, 27787 (1997).
33. S.-Z. Yan, Z.-H. Huang, R. S. Shaw, W.-J. Tang, *ibid.*, p. 12342.
34. F. Eckstein, P. Romaniuk, W. Heideman, D. Storm, *ibid.* **256**, 9118 (1981).
35. J. Gert, J. Coderre, M. Wolin, *ibid.* **255**, 331 (1980).
36. K. Koch, F. Eckstein, L. Stryer, *ibid.* **265**, 9659 (1990).
37. P. Senter, F. Eckstein, A. Mulsch, E. Bohme, *ibid.* **258**, 6741 (1983).
38. G. Zhang *et al.*, *Protein Sci.* **6**, 903 (1997).
39. J. Sonddek, D. G. Lambright, J. P. Noel, H. E. Hamm, P. B. Sigler, *Nature* **372**, 276 (1994).
40. J. Perona, M. A. Rould, T. A. Steitz, *Biochemistry* **32**, 8758 (1993).
41. T. Schweins *et al.*, *Nature Struct. Biol.* **2**, 36 (1995).
42. P. J. Artymiuk, A. R. Poirrette, D. W. Rice, P. Willett, *Nature* **388**, 33 (1997).
43. T. A. Steitz, S. J. Smerdon, J. Jäger, C. M. Joyce, *Science* **266**, 2022 (1994).
44. Z. Otwinowski, in *Data Collection and Processing*, N. I. L. Sawyer, and S. Bailey, Eds. (Science and Engineering Research Council Daresbury Laboratory, Daresbury, UK, 1993), pp. 56-62.
45. J. Navaza, *Acta Crystallogr.* **A50**, 157 (1994).
46. S. Bailey, *ibid.* **D50**, 760 (1994).
47. T. A. Jones, J. Y. Zou, S. W. Cowan, M. Kjeldgaard, *ibid.* **A47**, 110 (1991).
48. A. T. Brünger, *X-PLOR Version 3.1. A System for X-ray Crystallography and NMR* (Yale Univ. Press, New Haven and London, 1992).
49. R. A. Laskowski, M. W. MacArthur, D. S. Moss, J. M. Thornton, *J. Appl. Crystallogr.* **26**, 283 (1993).
50. Single-letter abbreviations for the amino acid residues are as follows: A, Ala; C, Cys; D, Asp; E, Glu; F, Phe; G, Gly; H, His; I, Ile; K, Lys; L, Leu; M, Met; N, Asn; P, Pro; Q, Gln; R, Arg; S, Ser; T, Thr; V, Val; W, Trp; and Y, Tyr.
51. R. M. Esnouf, *J. Mol. Graphics* **15**, 133 (1997).
52. E. A. Merritt and E. P. Murphy, *Acta Crystallogr.* **D50**, 869 (1994).
53. M. Nakane *et al.*, *J. Biol. Chem.* **265**, 16841 (1990).
54. P. G. Feinstein *et al.*, *Proc. Natl. Acad. Sci. U.S.A.* **88**, 10173 (1991).
55. Y. Ishikawa *et al.*, *J. Biol. Chem.* **267**, 13553 (1992).
56. We thank J. Collins for technical assistance; C. Dessauer for helpful discussion; D. Coleman, T. Harrell, T. Xiao, and the MacCHESS staff for assistance with data collection at CHESS; L. Esser for assistance in preparing figures; J. Hurley for providing the coordinates of the IIC₂ homodimer before their release in the Protein Data Bank; R. Johnson for supplying 2'-deoxy-3'-ATP (synthesis supported by NIH grant DK38828); and R. Cooke for supplying 2'-iodo-ATP. Supported by NIH grant DK46371 and Welch Foundation grant I-1229 to S.R.S.; by NIH grant GM34497, American Cancer Society grant RPG-77-001-21-BE, Welch Foundation grant I-1271, and the Raymond and Ellen Willie Distinguished Chair of Molecular Neuropharmacology to A.G.G.; and a postdoctoral fellowship from the Medical Research Council of Canada to R.K.S. Atomic coordinates have been submitted to the Protein Data Bank (1AZS).

24 October 1997; accepted 14 November 1997